J. Fluid Mech. (2000), *vol.* 404, *pp.* 269–287. Printed in the United Kingdom

Instabilities of exact, time-periodic solutions of the incompressible Euler equations

By JOSEPH A. BIELLO[1], KENNETH I. SALDANHA[2] AND NORMAN R. LEBOVITZ[2]

[1]Department of Astronomy and Astrophysics, University of Chicago, Chicago, IL 60637, USA
[2]Department of Mathematics, The University of Chicago, Chicago, IL 60637, USA

(Received 27 May 1999 and in revised form 28 August 1999)

We consider the linear stability of exact, temporally periodic solutions of the Euler equations of incompressible, inviscid flow in an ellipsoidal domain. The problem of linear stability is reduced, without approximation, to a hierarchy of finite-dimensional Floquet problems governing fluid-dynamical perturbations of differing spatial scales and symmetries. We study two of these Floquet problems in detail, emphasizing parameter regimes of special physical significance. One of these regimes includes periodic flows differing only slightly from steady flows. Another includes long-period flows representing the nonlinear outcome of an instability of steady flows. In both cases much of the parameter space corresponds to instability, excepting a region adjacent to the spherical configuration. In the second case, even if the ellipsoid departs only moderately from a sphere, there are filamentary regions of instability in the parameter space. We relate this and other features of our results to properties of reversible and Hamiltonian systems, and compare our results with related studies of periodic flows.

1. Introduction

In this paper we study the stability of a family of exact, temporally periodic solutions of the Euler equations governing an inviscid, incompressible fluid. These equations are

$$\left.\begin{aligned} \boldsymbol{u}_t + \boldsymbol{u}\cdot\nabla\boldsymbol{u} + \nabla p = 0, \\ \nabla\cdot\boldsymbol{u} = 0, \\ \hat{\boldsymbol{n}}\cdot\boldsymbol{u}|_{\partial D} = 0. \end{aligned}\right\} \tag{1.1}$$

We consider an ellipsoidal domain D fixed in the inertial frame,

$$D = \left\{ \boldsymbol{x} \Big| \sum_{i=1}^{3} \left(\frac{x_i}{a_i}\right)^2 \leqslant 1 \right\}.$$

These equations possess the 'simple motion' solution in the terminology of Poincaré (1910) for a flow linear in the Cartesian coordinates,

$$\boldsymbol{u} = \begin{pmatrix} 0 & -\dfrac{a_1}{a_2}m_3 & \dfrac{a_1}{a_3}m_2 \\ \dfrac{a_2}{a_1}m_3 & 0 & -\dfrac{a_2}{a_3}m_1 \\ -\dfrac{a_3}{a_1}m_2 & \dfrac{a_3}{a_2}m_1 & 0 \end{pmatrix} \boldsymbol{x}, \tag{1.2}$$

provided the coefficients m_1, m_2, m_3 satisfy the following system of ordinary differential equations:

$$I_1\dot{m}_1 = (I_3 - I_2)m_2m_3, \quad I_2\dot{m}_2 = (I_1 - I_3)m_1m_3, \quad I_3\dot{m}_3 = (I_2 - I_1)m_1m_2, \tag{1.3}$$

where $I_1 = a_2^2 + a_3^2$, $I_2 = a_3^2 + a_1^2$, $I_3 = a_1^2 + a_2^2$. These equations are, except for an inessential sign change, identical with those governing the dynamics of a rigid body. Their solutions are well understood. All orbits are periodic and, therefore, for any choice of initial data, they provide a temporally periodic solution of the equations of inviscid fluid dynamics, the spatial structure being provided by equation (1.2). Since the velocity field is linear in the Cartesian coordinates, the motion in question has, at any instant of time, uniform vorticity, but which varies periodically with time. In this paper we study the stability of these temporally periodic velocity fields.

Forster & Craik (1996) have undertaken a similar study in the case when the fluid occupies all of space so that the boundary condition in equation (1.1) can be ignored. Their method exploits the circumstance that the linearized Euler equations have solutions in the form of time-dependent plane waves. To apply these results to the bounded case, one limits the wavenumbers to those that are 'sufficiently large' so that localized wave packets of small wavelength can develop without being influenced by the boundary. From the standpoint of examining the stability of these periodic solutions in the bounded domain, that work therefore provides the limit of disturbances of asymptotically small spatial scale. By contrast, the method employed in the present paper, while in principle applicable to all spatial scales, is only practicable for large to moderate spatial scales. These methods are therefore complementary.

Viscosity is neglected in the present paper but in applications to laboratory, planetary or astrophysical flows, its effects need to be considered. The solution (1.2) of the Euler equations is likewise a solution of the Navier–Stokes equations but fails to be a solution of the viscous problem because it does not satisfy the no-slip boundary condition. It is therefore a leading contender for an outer solution of the viscous problem via boundary-layer theory. Although there has been no boundary-layer analysis for this problem, the analysis of Roberts & Stewartson (1965), as amended in Busse (1968), in the analogous problem of flow in a precessing spheroid has confirmed that the analogous simple motion of Poincaré (1910) (cf. §4.2) indeed represents an approximate outer solution for that problem. Motion very much like that described by the solution (1.2) is found in the laboratory experiments of Gledzer *et al.* (1974). Where stability theory is concerned, viscosity damps the elliptic instability in the short-wave limit. This damping is less effective for the perturbations of large to moderate spatial scale considered here, so these are the inviscid motions most likely to persist in the presence of viscosity. Even these must be modified by viscosity through the effect of boundary layers. However, experience with related problems, including laboratory experiments (cf. Kerswell 1993; Gledzer & Ponomarev 1992; Malkus 1989)

suggest that, when the inviscid equations predict an inertial instability of sufficiently large growth rate, the conclusion of instability persists in the presence of viscosity.

A principal physical motivation for the present study derives from studies of the *elliptic instability*. This refers to the widespread instability of the planar flow

$$\boldsymbol{u} = c\left(-\frac{a_1}{a_2}x_2, \frac{a_2}{a_1}x_1, 0\right). \tag{1.4}$$

For any choice of the constant c this is an equilibrium solution of the Euler equations if the cross-sections in the (x_1x_2)-plane of the domain D are ellipses with semiaxes a_1 and a_2 (or if the domain is all of space). If $a_2 = a_1$ this is a rigid-body rotation and is stable in most applications where it arises. However, if $a_2 \neq a_1$, the streamlines are ellipses, and it is in many cases unstable. In the unbounded case, it is 'universally' unstable, which is to say that in the absence of other effects (like rotation, for example) it is unstable without any qualification (Pierrehumbert 1986; Bayly 1986; Waleffe 1990). In the bounded case, where a normal-mode analysis can be used, the various normal modes may or may not predict instability, depending on the domain (see, for example, Gledzer & Ponomarev 1992 for a review of this problem). In the cases of ellipsoids or elliptic cylinders, which have been studied in the laboratory, the aspect ratios are the critical parameters for determining instability for specific normal modes. It is plausible that if all normal modes are taken into account, and if the fluid could be considered strictly inviscid, the instability would be universal also in the case of bounded domains, i.e. would hold irrespective of the axes ratios. Laboratory experiments do not confirm this picture; there are parameter regions of stability as well as of instability. These can be related to the theoretically derived instabilities of normal modes of rather low order (i.e. of moderate to large spatial scales).

Most of the theoretical research on the elliptic instability for bounded domains has been directed at the linearized stability problem, although there have been a few efforts in the direction of weakly nonlinear approximations as well (cf. Gledzer & Ponomarev 1977; Waleffe 1989; Guckenheimer & Mahalov 1992; Knobloch, Mahalov & Marsden 1994; Lebovitz & Saldanha 1999). Understanding the nature of the nonlinear flow that develops in consequence of the elliptic instability is of considerable interest both in laboratory and in natural settings. Recently Kerswell (1999) and Mason & Kerswell (1999) have studied the stability of flows that are near the basic flow with elliptic streamlines (i.e. similar to (1.4)). Their stability analysis is carried out for a flow which arises from the saturation of a pair of unstable inertial waves superposed on the elliptic flow, i.e. they are investigating the secondary instabilities of the underlying elliptic flow. Their analysis requires the saturation of the primary instability at a small amplitude. However, it was emphasized in Lebovitz & Saldanha (1999) that saturation at small amplitude may be an exceptional case: most of the bifurcations studied there fail to saturate at small amplitude. This complicates finding the flows from which a secondary flow may bifurcate. The time-periodic solutions of the Euler equations (1.2) and (1.3) above provide a natural opportunity to realize such an exact nonlinear development, in the following way. If we supply (1.3) with initial data $(m_1, m_2, m_3) = (0, 0, c)$, the corresponding velocity field is precisely the steady elliptic flow (1.4). This is unstable if a_3 is intermediate in size between a_1 and a_2 (since this makes I_3 the intermediate moment of inertia), to perturbations that leave the velocity field in the simple form given by equation (1.2). The nonlinear outcome of a perturbation in this class of perturbations is therefore one of the periodic orbits studied here. Experiments intended to check this seem to confirm it (Gledzer *et al.* 1974), at least for the (extremely) short times for which the outcome could be observed. This

is one of our motivations for studying the stability of these periodic solutions, and it governs the choice of one of the parameter regimes that we explore.

As Forster & Craik (1996) point out, this problem may be the only one in the hydrodynamic literature to consider the stability of a three-dimensional, periodic flow that is not reducible to a steady flow in a rotating frame. However, in the special case when two semiaxes are equal, it is possible to transform to a frame in which the motion is steady, and there are then similarities to Poincaré's solution for a precessing fluid spheroid. The stability problem for that case has been considered by Kerswell (1993). We compare the two stability problems.

Our technique is based on the following property of the linear stability problem: it decomposes into an infinite hierarchy of finite-dimensional problems, each providing an exact solution of the original stability problem. This in turn is a consequence of the invariance of spaces of vector polynomials under the linear operator appearing in the stability problem. The two lowest-degree spaces, of degrees eight and eighteen, correspond to fluid motions on the scale (roughly) of one-half and one-third the size of the domain, respectively. These are the ones we investigate in detail in this paper, although there is no obstacle in principle to considering further systems in the hierarchy.

The plan of the paper is as follows. In § 2 we describe the parameter space of periodic solutions, present the linearized equations, and explain the technique for analysing them. The results of the numerical solutions of the resulting Floquet problems are presented and interpreted in § 3. There is a discussion of these results and their relation with previous research in § 4.

2. Formulation

2.1. *The unperturbed periodic solutions*

We need to parametrize the periodic orbits. There are three semi-axes and three choices of initial data for the system (1.3), but we do not need six parameters: three suffice. It is clear from (1.3) that only the ratios of the semi-axes enter into the problem. Furthermore, permuting the semi-axes a_i cyclically and carrying out the same cyclic permutation on the dynamic variables m_i leaves the equations unchanged. Using these invariances we can choose, without loss of generality, the following ordering of the semi-axes:

$$a_2 < a_1 = 1 < a_3. \tag{2.1}$$

This makes the a_1 semi-axis the intermediate one so, if we wish to study the periodic solutions representing the nonlinear development of the elliptic instability, we consider perturbations of the steady solution with vorticity in this direction. We now rewrite (1.3), letting $m_1 \to -a_2 a_3 m_1/2$, $m_2 \to -a_3 a_1 m_2/2$ and $m_3 \to -a_1 a_2 m_3/2$:

$$\dot{m}_1 = K_1^2 m_2 m_3, \quad \dot{m}_2 = -K_2^2 m_1 m_3, \quad \dot{m}_3 = -K_3^2 m_1 m_2. \tag{2.2}$$

Here

$$K_1 = \left[\frac{2(a_3^2 - a_2^2)}{a_2^2 + a_3^2}\right]^{1/2}, \qquad K_2 = \left[\frac{2(a_3^2 - 1)}{a_2^2(1 + a_3^2)}\right]^{1/2}, \qquad K_3 = \left[\frac{2(1 - a_2^2)}{a_3^2(1 + a_2^2)}\right]^{1/2}.$$

Setting $\tilde{m}_i = r m_i$, with r a constant and rescaling time by $\tau = t/r$ leaves the system unchanged. The scale factor r is chosen implicitly in equations (2.3) below. Rescaling therefore eliminates two of the original six parameters. We can eliminate one more by appropriate labelling of orbits, as follows.

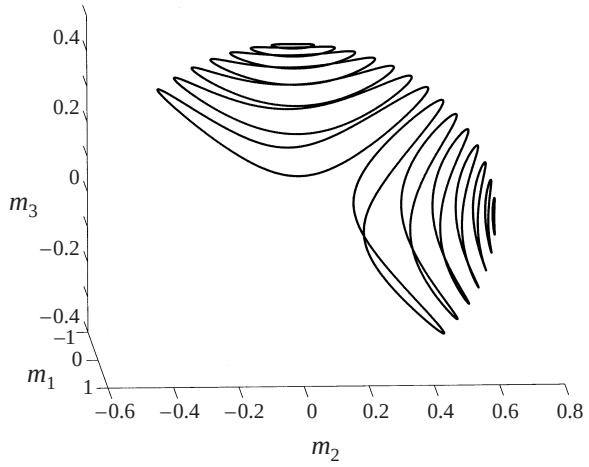

FIGURE 1. Setting $a_1 = 1, a_2 = 0.85$ and $a_3 = 1.15$ we numerically compute a sampling of solutions of (2.2) for initial conditions along the contour $\mathscr{C}$ described in (2.3).

Consider solutions of (2.2). The fixed points, aside from the origin, which do not interest us, are $\overline{m_1}, \overline{m_2}$ and $\overline{m_3}$ where $\overline{m_1} = (m_1^0, 0, 0)$, the other two points being defined analogously. From the expression (1.2) it is clear that each fixed point of (2.2) is associated with a steady solution of (1.1). Equation (2.2) has two conserved quantities, which we choose in the form

$$\Gamma_1^2 = \left(\frac{m_1}{K_1}\right)^2 + \left(\frac{m_2}{K_2}\right)^2 \quad \text{and} \quad \Gamma_2^2 = \left(\frac{m_1}{K_1}\right)^2 + \left(\frac{m_3}{K_3}\right)^2.$$

In the (m_1, m_2, m_3) phase space, the surfaces of constant Γ_1^2 and Γ_2^2 are elliptic cylinders centred about the m_3 and m_2 axis respectively. Solutions of the system must lie on the intersections of these two invariant surfaces, and may be described by the relative values of Γ_1 and Γ_2. Setting $\Gamma_1 = 0$ produces the equilibrium point $\overline{m_3}$, and setting $\Gamma_2 = 0$ produces the equilibrium $\overline{m_2}$. When $\Gamma_1 \ll \Gamma_2$ (i.e. when the elliptic cylinder about the m_3-axis is much thinner than the one about the m_2-axis), solutions execute small oscillations about $\overline{m_3}$. Analogously, $\Gamma_2 \ll \Gamma_1$ produces orbits that execute small oscillations about $\overline{m_2}$. Changing the relative values of the Γ_i smoothly will smoothly deform these orbits into wider oscillations. This deformation can be carried out (from either extreme value) up to the critical value $\Gamma_1 = \Gamma_2$ (i.e. choosing initial conditions $m_2^0/K_2 = m_3^0/K_3$). At this critical value the two conserved quantities are not independent in the neighbourhood of the (hyperbolic) fixed point $\overline{m_1}$, and the solution produced by the intersection of the invariant surfaces is a separatrix orbit passing through this point. Figure 1 shows a numerically computed sampling of the orbits described above. Recall the scale invariance of the dynamical variables; in particular, choosing $r = -1$ will produce the qualitatively equivalent orbits in the other octants, which are not depicted in the figure. Changing the relative values of Γ_1 and Γ_2 can be achieved through a single parameterization. In figure 1, consider the 'half-longitude' on the plane $m_1 = 0$ that connects the equilibrium points $\overline{m_2}$ and $\overline{m_3}$. This one-dimensional curve $\mathscr{C}$, which passes through all orbits on the hemisphere, can be described by a single parameter θ:

$$\boldsymbol{m}(0) = (0, K_2 \sin(\theta), K_3 \cos(\theta)), \quad 0 \leqslant \theta \leqslant \pi/2. \tag{2.3}$$

At $\theta = 0$ this parameterization sets $(\Gamma_1, \Gamma_2) = (0, 1)$, picking out the equilibrium point $\overline{m_3}$, and as θ increases smoothly it varies the relative values of Γ_1 and Γ_2, ending at $(\Gamma_1, \Gamma_2) = (1, 0)$ (i.e. at $\overline{m_2}$) when $\theta = \pi/2$. The separatrix orbit is crossed at $\theta = \pi/4$.

To summarize, on the basis of the symmetries of the system (1.3) with respect to the semi-axes $\{a_i\}$ as well as the dynamic variables $\{m_i\}$, we obtain all possible periodic orbits of the system by fixing the ordering of the semi-axes as in (2.1) and considering orbits produced from initial conditions along the contour $\mathscr{C}$.

2.2. *The perturbed problem*

Let us suppose that we now have a periodic solution $\boldsymbol{u}$ to Euler's equation for fluid flow. Let $\boldsymbol{v}$ be a small perturbation to $\boldsymbol{u}$. The linearized evolution equation governing $\boldsymbol{v}$ is

$$\boldsymbol{v}_t + L\boldsymbol{v} = -\nabla p, \tag{2.4}$$

where p now denotes the pressure perturbation and

$$L\boldsymbol{v} = \boldsymbol{u} \cdot \nabla \boldsymbol{v} + \boldsymbol{v} \cdot \nabla \boldsymbol{u}. \tag{2.5}$$

Consider the action of L on a vector polynomial, by which we mean a vector $\boldsymbol{v}$ for which each component v_1, v_2, v_3 is a polynomial in the Cartesian coordinates. Denote by n the maximum of the degrees of the three component polynomials; we shall refer to this as the degree of $\boldsymbol{v}$. Since $\boldsymbol{u}$ itself has this form with $n = 1$, it is obvious from equation (2.5) that $L\boldsymbol{v}$ is also a vector polynomial of the same degree. Vector polynomials of given degree form a finite-dimensional linear space, so this observation can be restated: L acts invariantly on polynomial spaces of given degree. This invariance extends to the projection of L onto the linear space defined by $\operatorname{div} \boldsymbol{v} = 0$, $\boldsymbol{v} \cdot \boldsymbol{n} = 0$ on the boundary (Lebovitz 1989). This is the underlying reason why the linear stability problem decomposes exactly into a hierarchy of finite-dimensional problems.

In exploiting this property by expanding the solutions in polynomials, we need also to impose the remaining conditions that $\operatorname{div} \boldsymbol{v} = 0$ in D and $\boldsymbol{v} \cdot \boldsymbol{n} = 0$ on ∂D. However, this can also be achieved by constructing a basis of vector polynomials $\{\boldsymbol{\eta}_i\}_1^\infty$ satisfying these conditions. Such a basis has been constructed (Lebovitz 1989). The basis functions of degree one, for example, may be written

$$\boldsymbol{\eta}_1 = \begin{pmatrix} 0 \\ -a_2 x_3/a_3 \\ a_3 x_2/a_2 \end{pmatrix}, \quad \boldsymbol{\eta}_2 = \begin{pmatrix} a_1 x_3/a_3, \\ 0 \\ -a_3 x_1/a_1 \end{pmatrix}, \quad \boldsymbol{\eta}_3 = \begin{pmatrix} -a_1 x_2/a_2 \\ a_2 x_1/a_1 \\ 0 \end{pmatrix}. \tag{2.6}$$

The unperturbed velocity field (1.2) can alternatively be expressed in the form $\boldsymbol{u} = \sum_1^3 m_i(t)\boldsymbol{\eta}_i$. The basis is not orthonormal† as given in Lebovitz (1989) but can be orthonormalized and we shall assume in the discussion below that this has been done.

By the reasoning described above, there exist exact solutions of equation (2.4) in the form

$$\boldsymbol{v}(x, t) = \sum \alpha_i(t)\boldsymbol{\eta}_i(\boldsymbol{x}), \tag{2.7}$$

where the sum goes over indices belonging to the basis vectors $\{\boldsymbol{\eta}_i\}$ of a prescribed maximal degree. Substitution in equation (2.4) then results in the finite-dimensional system

$$\frac{\mathrm{d}\boldsymbol{\alpha}}{\mathrm{d}t} + \mathscr{L}\boldsymbol{\alpha} = 0 \tag{2.8}$$

† We use the standard inner product $\langle \boldsymbol{u}, \boldsymbol{v} \rangle = \int_D \boldsymbol{u}(\boldsymbol{x}) \cdot \boldsymbol{v}(\boldsymbol{x})\, \mathrm{d}\boldsymbol{x}$.

where the matrix $\mathscr{L}$ is defined by

$$(\mathscr{L})_{jk} = \langle \eta_j, L\eta_k \rangle \tag{2.9}$$

and the indices j and k run over the same set as in equation (2.7). Matrices $\mathscr{L}$ obtained in this way are periodic with the period T of the unperturbed orbit, so a hierarchy of Floquet problems is obtained in this way. We treat in detail the two that correspond to the lowest polynomial degrees, two and three, which turn out to be of dimensions eight and eighteen, respectively. The numerical treatment of these Floquet problems is routine, but has a special feature to which we wish to draw attention.

2.3. *Reversibility*

The treatment of the Floquet problem proceeds by constructing a Floquet multiplier matrix $\boldsymbol{M}$ and checking to see whether any eigenvalue has modulus exceeding unity. In doing this we have found that the eigenvalues come in quartets $\lambda, \bar{\lambda}, 1/\lambda, 1/\bar{\lambda}$, where the overbar signifies the complex conjugate. This is the pattern for symplectic maps, such as one would derive from a canonical, Hamiltonian system, but our systems are not Hamiltonian.† We find, however, that the periodic differential equations (2.8) are reversible. This means that there is an operator R with $R^2 = I$ such that $R\mathscr{L}(t) = -\mathscr{L}(-t)R$. For the Floquet matrix $\boldsymbol{M}$ this implies that $R\boldsymbol{M} = \boldsymbol{M}^{-1}R$. This reversibility suffices to explain the quartet structure for the eigenvalues, since it implies that whenever λ is an eigenvalue, so is λ^{-1}.

We omit the proof since it is somewhat lengthy and is tangential to our main purpose.

3. Results

We carry out the numerical computation of the Floquet multipliers for perturbations $\boldsymbol{v}$ expressed by basis functions whose components are quadratic and cubic polynomials. Since the argument showing the reduction of the problem to finite dimensions relied only on the invariance of polynomial spaces of maximal degree under the action of L, it might be thought that the system arising in the quadratic case would appear again as a subsystem in the cubic case. However, because of further symmetries (Lebovitz 1989), terms of even and of odd degrees are uncoupled, and the two systems we describe here are therefore uncoupled.

The equations (2.2), which produce the unperturbed, periodic solution, require a choice of the parameters a_2, a_3, θ. These then determine the operator L, but to define the matrix $\mathscr{L}$ figuring in the Floquet theory, we need to perform the integrations implicit in the definition (2.9). These, however, can be carried out exactly since the integrands are polynomials in the Cartesian coordinates. We produce the periodic matrices $\mathscr{L}$ in this way. We then construct the Floquet matrix $\boldsymbol{M}(T)$ numerically. The background orbit is unstable if there exists λ_i, an eigenvalue of $\boldsymbol{M}(T)$, such that $|\lambda_i| > 1$. It is related to the growth rate g_i by the formula

$$g_i = \frac{\ln(|\lambda_i|)}{T}. \tag{3.1}$$

For each of the two classes of perturbations, we investigate the stability of two qualitatively different classes of periodic orbits:

† There are indications (Morrison 1998) that systems derived in this way are generically non-Hamiltonian even if the underlying system has a Hamiltonian character.

(*a*) those executing small oscillations about a nearby equilibrium solution (to test the robustness of the conclusions of elliptic-instability theory), and

(*b*) near-separatrix orbits that execute large oscillations with significant excursions from their initial conditions (representing the exact nonlinear outcome of a small perturbation of an unstable steady solution).

3.1. *Near-equilibrium orbits*

Choosing $\theta = 0^+$ sets $\boldsymbol{m}^0 = (0, 0^+, 1^-)$ and produces a periodic orbit that is dominated by the steady solution $\boldsymbol{\eta}_3$. In the fluid dynamical context, this produces a periodic velocity field which has vorticity primarily in the x_3-direction (we recall that a_3 is the largest semi-axis; we refer to this as the prolate case). On the other hand, $\theta = (\pi/2)^-$ sets $\boldsymbol{m}^0 = (0, 1^-, 0^+)$, producing an orbit dominated by the steady solution η_2. In this case, the vorticity of the periodic solution in the fluid context is primarily in the x_2-direction (a_2 is the smallest semi-axis; the oblate case). In our computations we set $\theta = 0.02$ for the first case and $\theta = 1.55$ for the second. In figure 1, these are the orbits close to the 'north pole' and 'east pole' of the ellipsoidal domain, respectively. We expect the stability characteristics of such orbits to be dominated by the stability characteristics of the nearby equilibrium solutions. The latter have been the subject of previous investigations, which are therefore available for comparison. Our comparisons are with the stability investigation of Lebovitz & Saldanha (1999).

We first set $\theta = 0^+$. Figure 2 compares the stability of steady solutions with that of nearby periodic solutions, for perturbations represented by quadratic and cubic basis functions. The jagged boundaries in the figure are artifacts of the coarseness of the mesh over the computational domain.

We see that in the parameter regime adjacent to that of spherical symmetry, the stability characteristics of the equilibrium solution are well preserved by the nearby periodic solutions. There is a neighbourhood about spherical symmetry in which the periodic orbits are stable to the perturbations considered. In the parameter regime where both the periodic and equilibrium solutions are unstable, the largest eigenvalue is both of the same order of magnitude in modulus, and of the same complex phase: in both cases the critical eigenvalue is real.

Farther from the spherical configuration – at the upper parts of the frames shown in figure 2 – there are significant differences between the equilibrium and periodic orbits. This is particularly evident with respect to the response to the cubic perturbations (frame *d*), but is true as well for the quadratic perturbations (frame *c*). The upper right-hand region of this frame now corresponds to unstable periodic orbits. These instabilities are clearly associated with the time-dependence of the unperturbed flow.

For the cubic perturbations, there is a large augmentation of the unstable region in parameter space. The kink in the contours running through figure 2(*d*) indicates that for the more elliptical figures (intermediate a_2 values) a new instability associated with the periodic solutions acquires a growth rate surpassing that of the instability of the corresponding equilibrium solutions and persists for highly elongated figures. The growth rates for the cubic perturbations surpass those for the quadratic perturbations for highly elongated prolate figures (i.e. large a_3 and intermediate values of a_2).

Turning to the case $\theta = (\pi/2)^-$, we consider the stability of periodic orbits dominated by the equilibrium $\boldsymbol{\eta}_2$. Under our ordering, this equilibrium solution rotates about the minor axis of the ellipsoidal domain. Again, the stability diagrams of the equilibrium solutions are taken from Lebovitz & Saldanha (1999) and are reproduced in figure 3.

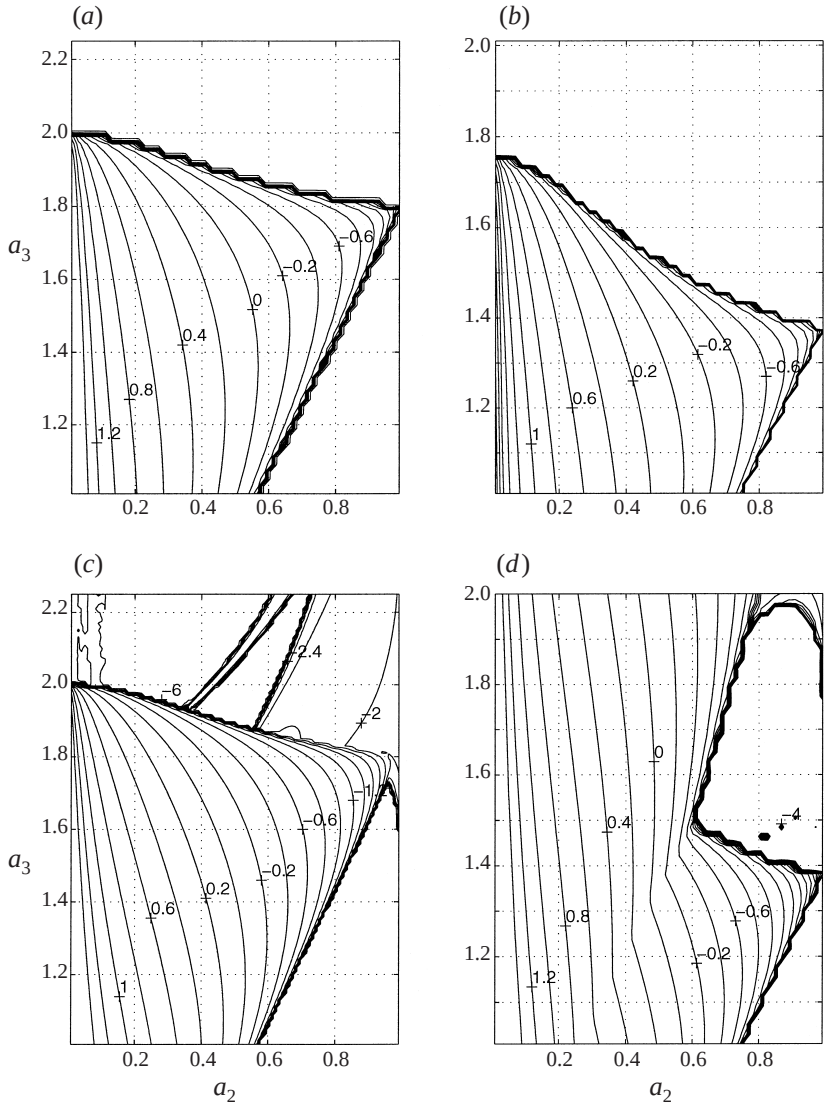

FIGURE 2. Contours of $\log(\mathrm{MAX}[g_i])$. (a, b) Reproductions of the instabilities of the steady solution η_3 to quadratic and cubic perturbations respectively, computed in Lebovitz & Saldanha (1999). (c, d) The instabilities of periodic solutions executing small oscillations about the steady solution. The (right) vertical axis represents a prolate spheroid, with $a_1 = a_2 < a_3$, and the spherically symmetric domain occurs at the lower right corner.

Here the periodic orbits tend once again to inherit the instability of the nearby equilibrium solution (see figure 3). For both quadratic and cubic perturbations, we also find an additional, narrow region of parameter space to be unstable. This is due to a strain component of the background flow in a direction perpendicular to that of the main fluid motion, i.e. the streamlines of the background flow are sheared normal to themselves. This instability is similar in origin to the inertial instabilities of Poincaré's precessing flow, as studied by Kerswell (1993). We discuss this more fully in § 4.2 below. This is likewise the origin of the narrow band of instabilities seen in the

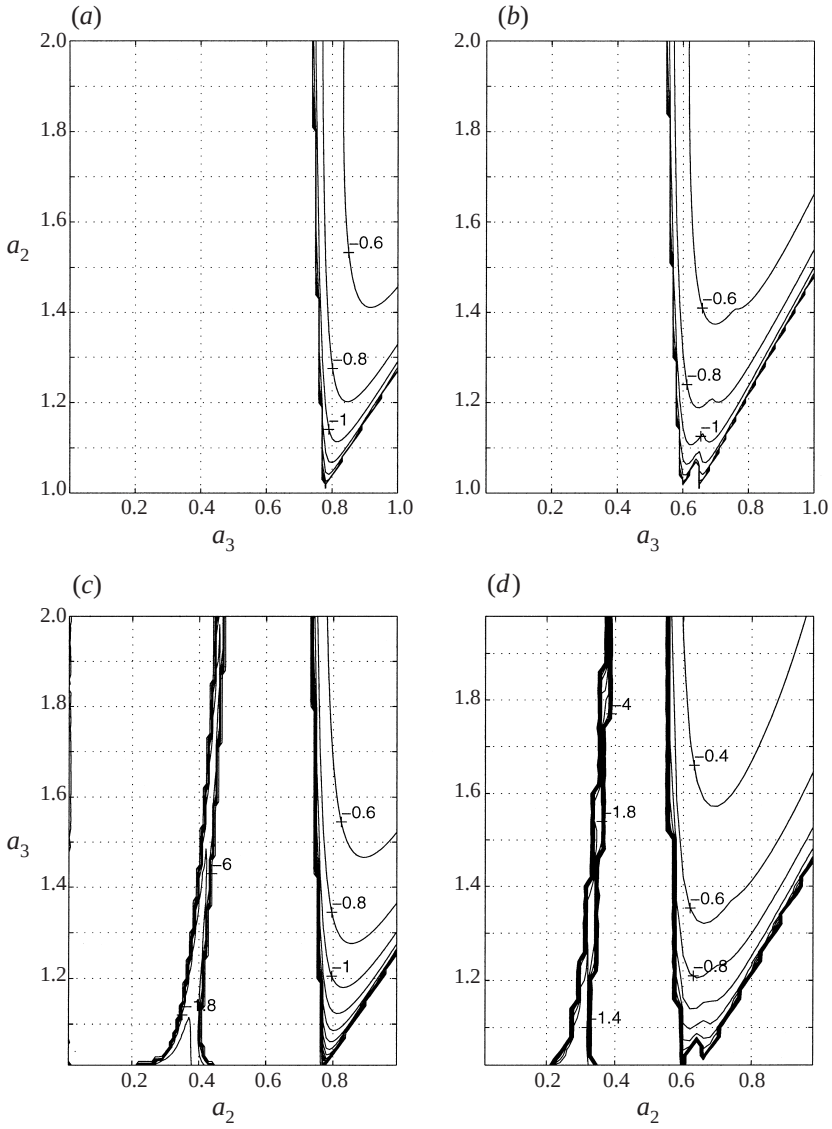

FIGURE 3. Contours of $\log(\mathrm{MAX}[g_i])$. (a, b) Reproductions of the instabilities of the steady solution η_2 to quadratic and cubic perturbations, respectively. (c, d) The unstable regions for periodic solutions executing small oscillations about the steady solution, to quadratic and cubic perturbations, respectively. The (bottom) horizontal axis represents an oblate spheroid ($a_1 = a_3 > a_2$) domain, with spherical symmetry occurring at the lower right corner.

upper centre of figure 2(*c*), and we believe that the additional parametric instabilities beyond those existing in the steady case have the same origin in some of the other cases as well, although we have only documented this in the two cases mentioned (see § 4.2).

In the region where the instability of the periodic solution is inherited from the corresponding nearby equilibria, the nature of the instability is likewise inherited: in this case both critical eigenvalues are complex.

3.2. *Near-separatrix orbits*

When a rigid body rotating about its intermediate axis is perturbed slightly, the ensuing motion takes place on the scale of the entire body, making extremely large, long-period excursions from the initial position. Regarded as a bifurcation problem, with parameter a_1 passing from the shortest axis (say) to the intermediate axis, it is a global bifurcation problem: the size of the new (periodic) solution is not limited by the difference between a_1 and its critical value. This likewise describes the periodic solutions governed by equations (1.2) and (1.3). The second class of orbits that we examine are precisely these near-separatrix orbits passing near the unstable steady solution. Such orbits are produced by setting $\theta \approx \pi/4$.

We first choose θ just less than $\pi/4$, so that the orbit in the $(m_1 m_2 m_3)$-space encloses the m_3-axis. The lengths of the periods of the unperturbed solutions increase as $\theta \to \pi/4$. In the case of quadratic perturbations, we use $\theta = 0.77$. However in the case of cubic perturbations, which is computationally far more expensive, we use $\theta = 0.75$ in order to decrease the numerical integrations required to produce each column of $\boldsymbol{M}(T)$. For perturbations approximated by quadratic and cubic basis functions, we find our chosen periodic orbit to be unstable in most of the parameter space. Figure 4 shows the computation of the growth rates for (a_2, a_3) on a relatively coarse mesh. This first computation suffices to indicate that there is a restricted region including the spherically symmetric configuration in which the orbits appear to remain stable. However, even this region – roughly $0.75 < a_2 \leqslant 1$, $1 \leqslant a_3 < 1.2$ – is not entirely stable.

In order to resolve the stability of the orbits in the small region about the spherically symmetric configuration, we refine our computations in this limited parameter regime. The results of these computations are shown in figure 5. The coarse structures seen in figure 4 now become well resolved into filaments of instability that striate this small region. Growth rates in the broader filaments are on the order of 10^{-3}, while in the finer filaments they shrink by orders of magnitude. Further refinements of the computational mesh in smaller regions of the parameter space produce further resolution of these filaments. We have by no means found all possible filaments of instability in our computations. The limiting values of reported growth rates g_i are chosen to be orders of magnitude higher than the error inherent in the numerical method. It is possible to set higher error tolerances for the integration and thus produce still finer filaments of instability.

Computations for $\theta > \pi/4$ (the orbit in the $m_1 m_2 m_3$-space encloses the east pole), specifically $\theta = 0.81$, indicate that there are no significant changes in the stability characteristics of a large oscillation orbit on the other side of the separatrix solution. Once again the parameter regime away from spherical symmetry refers to unstable orbits, and there are fine filaments of instability that striate the primarily stable regime close to spherical symmetry.

3.3. *The filamentary structures*

The filamentary structures can be understood qualitatively and related to those occurring in other conservative, dynamical problems. The periodic orbits passing near the unstable equilibrium solution remain close, in the $(m_1 m_2 m_3)$-space, to separatrix orbits heteroclinic to the unstable equilibrium points, their periods increasing without bound as they approach the separatrix. In a system with several degrees of freedom, there are other periods of motion associated with other degrees of freedom and, near the equilibrium point, these have bounded periods. The periods of the near-separatrix orbits must therefore pass through multiples of the latter as the separatrix

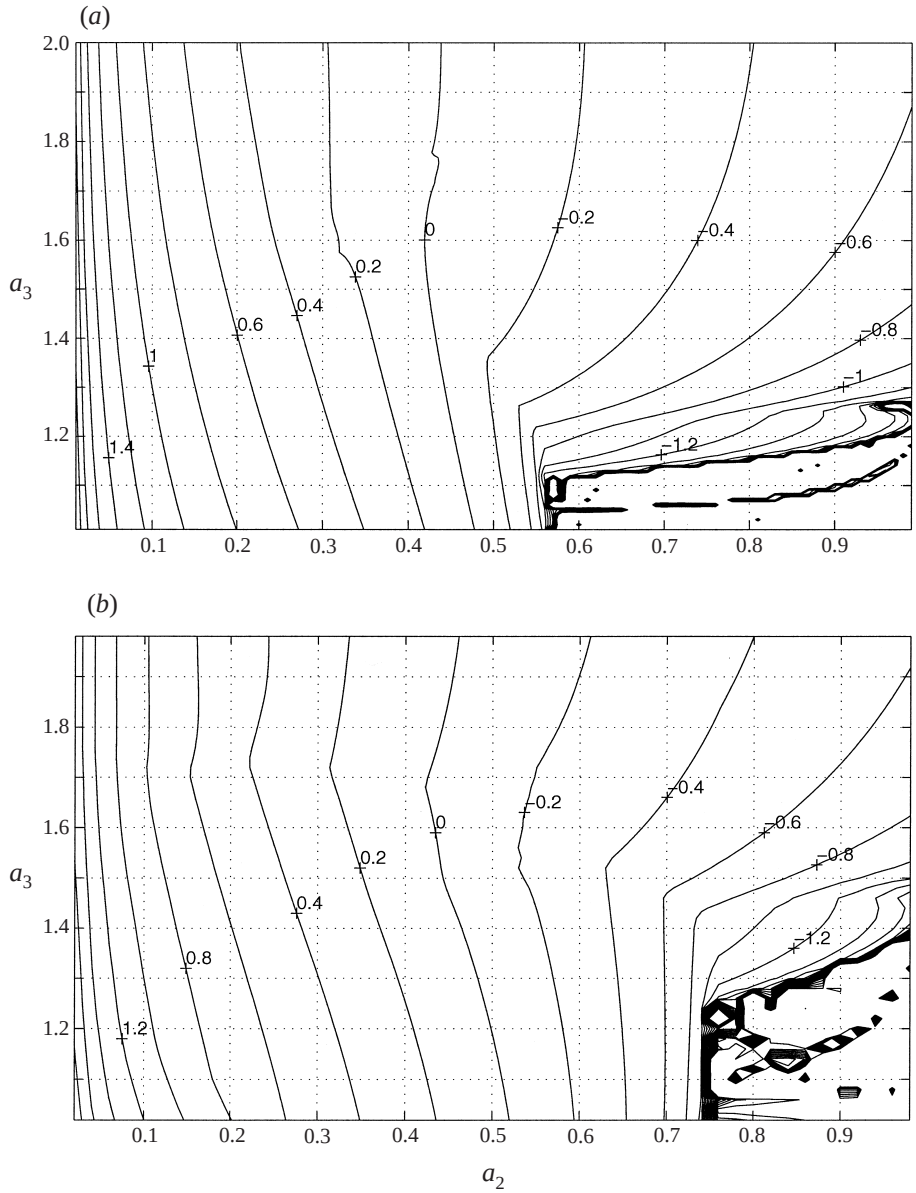

FIGURE 4. We fix $\theta = (\pi/4)^-$ so that the unperturbed periodic orbit executes large oscillations, rotating about the x_3-axis. With a relatively coarse mesh in (a_2, a_3), we find a restricted parameter regime close to the spherically symmetric configuration that has regions of stability. (*a*) Contours of $\log(g_i)$, for perturbations represented by quadratic polynomials, and (*b*) for cubic polynomials.

is approached, resulting in successive resonances that may mark the edges of bands of instability. This mechanism has been verified in some simple classes of Hamiltonian systems of two degrees of freedom by Churchill, Pecelli & Rod (1980).

To explore this numerically, we fix the semi-axes values of the domain, and take $\theta \to \pi/4$ (recall that $\theta = \pi/4$ represents the separatrix). Figure 6 shows the resultant growth rates as a function of orbital period. Only three bands are resolved in our calculations as longer periods take a very long time to compute and shorter periods,

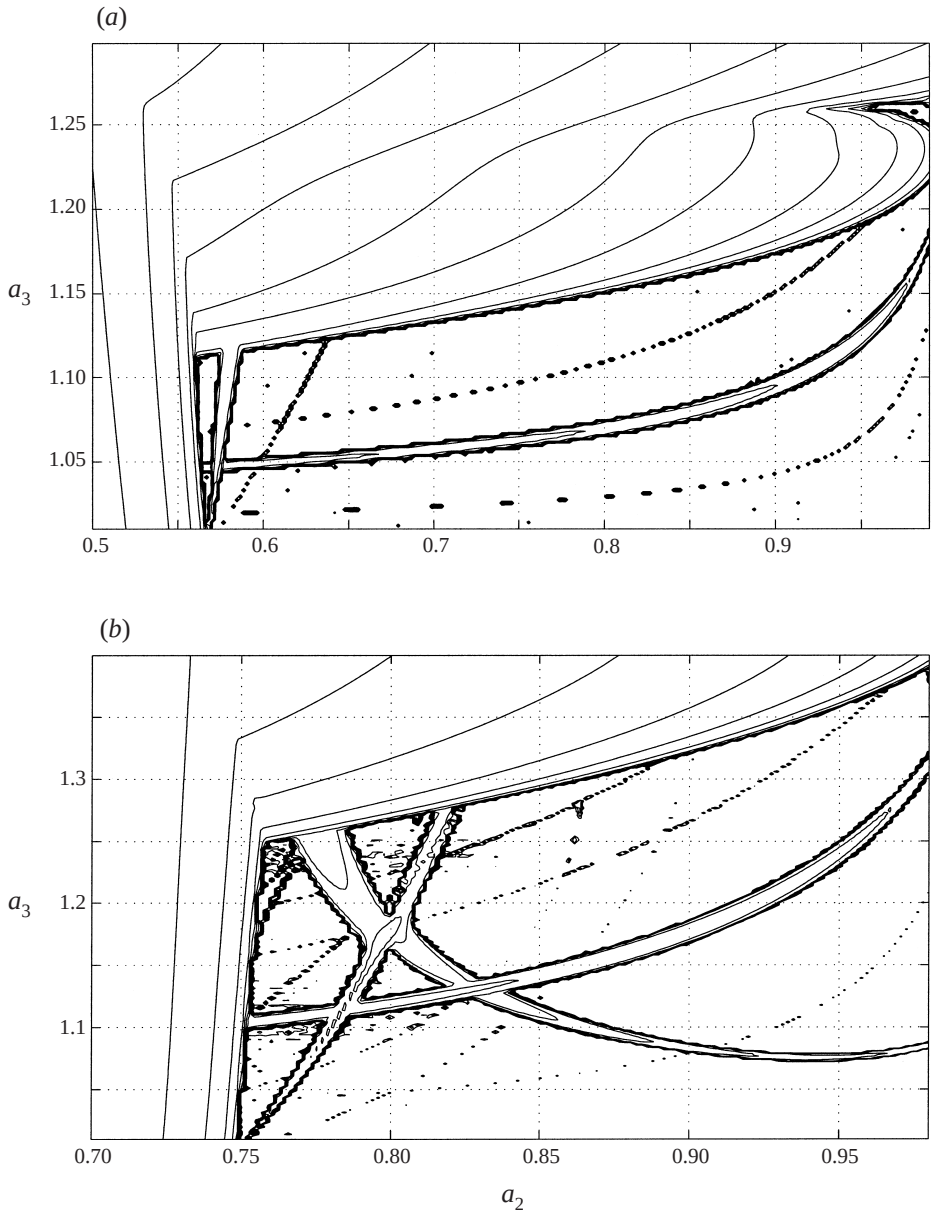

FIGURE 5. Refined computations in the parameter regime close to a spherically symmetric domain. The apparent island structures of the instabilities are filaments that are under-resolved by the current computational mesh. (*a*) Instability to perturbations represented by quadratic polynomials, and (*b*) for perturbations represented by cubic polynomials.

which occur farther from the separatrix, are no longer in the asymptotic regime where these bands are predicted (in order to capture these bands, we have taken θ within 10^{-7} of $\pi/4$). Among the features of the resonance mechanism explained above is that the distance between instability bands, as well as their widths, should be approximately constant when measured in terms of the periods of the near-separatrix orbits. Our computations are seen to be consistent with this mechanism. They further

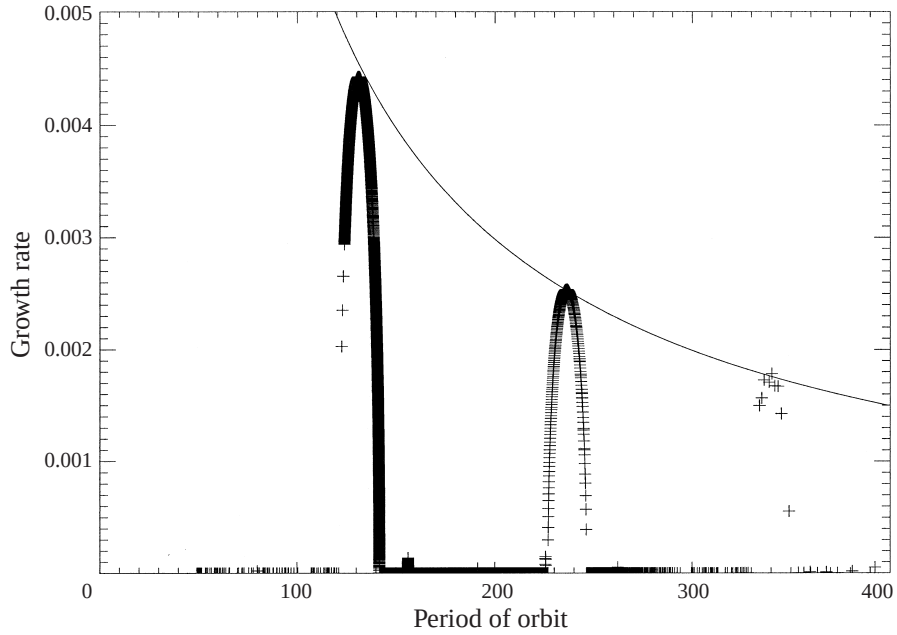

FIGURE 6. Growth rate as a function orbital period. Three unstable bands are resolved and a T^{-1} curve is plotted with arbitrary amplitude for comparison. For $T = 400$, the initial condition of the orbit is less than 10^{-7} away from the separatrix.

indicate that the maximum growth rate decays as T^{-1}, implying constancy of the eigenvalues of $\boldsymbol{M}$ (see equation (3.1)).

4. Discussion

We address two issues in this section: (i) our conclusions regarding the elliptic instability and their physical implications and (ii) the relation of the present work to that of Kerswell (1993), and conclude with a brief summary.

4.1. *The elliptic instability*

Consider first the case when the periodic solutions of the Euler equations described by equations (1.2) and (1.3) result from a perturbation of steady flow about the intermediate axis. These can represent the long-term outcome of the elliptic instability only for a relatively small range of axes values including figures not very highly distorted from the spherical. For axes values outside this range, the relevant periodic solutions are unstable. Even within this range there are narrow subregions of instability, represented by the filamentary structures in figures 4 and 5. Likewise, for the other parametric domains considered, the near-sphere region remains stable, but much of the remaining parameter space corresponds to unstable periodic solutions. Consideration of perturbations of smaller spatial scale than those considered in this paper can only have the effect of further constricting this region of stability. It may be that all such periodic solutions are unstable. However, there are caveats.

The near-sphere parameter domain represents a region of parameter space where instability of the periodic solutions has not been established (cf. figures 7(*a*) and 7(*b*) below). The investigation of Forster & Craik (1996) relates to the instability

of the periodic solutions governed by equations (1.2) and (1.3) to perturbations of asymptotically small spatial scale, but excludes the near-sphere region of parameter space. Even for the filamentary regions of instability seen in figures 4 and 5, the associated growth rates are small, so the corresponding orbits could persist for a long time despite a formal conclusion of instability. The near-sphere region is of special interest in natural settings such as those of planets, stars and galaxies. In their related study of the stability of the Riemann ellipsoids, Lebovitz & Lifschitz (1996) found this region of parameter space to be stable to perturbations both of large to moderate spatial scale and of asymptotically small spatial scale. For these reasons, it may be premature to disregard these simple flows as physically irrelevant.

Our test of the robustness of the conclusions of the elliptic-instability theory consisted in considering the stability of periodic solutions differing very little from steady solutions. In two of the four cases considered, the pattern of stability and instability of the steady solutions was essentially inherited by the nearby periodic solutions, with only a small augmentation in the parameter space corresponding to instability. In the remaining cases, however, the small change in the unperturbed solution resulted in a large augmentation in the region of instability. We tentatively conclude that the elliptic-instability theory underestimates the amount of parameter space in which these simple flows are unstable, since a small imperfection in the initial data (leading to a periodic rather than a steady unperturbed flow) increases the possibilities for instability.

4.2. *Relation to the Poincaré solutions*

There is a similarity between the flows considered here and those found by Poincaré (1910) as models for a precessing liquid planet. The stability of the latter has been considered by Kerswell (1993). There are equally important differences as well, and we address both the similarities and the differences here.

Poincaré's solution refers to a steady flow in a uniformly rotating reference frame in which the figure is a spheroid. In general the periodic solutions considered in this paper cannot be reduced to steady flow in a uniformly rotating frame, but there are exceptions: if the figure is a spheroid ($a_2 = a_1$, a_3 arbitrary), then such a reduction is possible. Moreover, this is an important limiting case for our analysis. When $a_2 = a_1 = 1$, the solution of the system (1.3) is

$$m_1 = A\cos(\Omega t + \alpha), \qquad m_2 = A\sin(\Omega t + \alpha), \qquad m_3 = \zeta, \tag{4.1}$$

where A, α, ζ are constants of integration and $\Omega = \left(1 - a_3^2\right)\zeta/2$. The corresponding velocity field, obtained from equation (1.2) is

$$\boldsymbol{u} = \begin{pmatrix} 0 & -\zeta & A\sin(\Omega t + \alpha)/a_3 \\ \zeta & 0 & -A\cos(\Omega t + \alpha)/a_3 \\ -a_3 A\sin(\Omega t + \alpha) & a_3 & 0 \end{pmatrix} \boldsymbol{x}. \tag{4.2}$$

This is expressed in Cartesian coordinates in the inertial frame. Define $\boldsymbol{R}(t)$ to be the rotation matrix about the $\hat{z}$-axis through the angle $\Omega t + \alpha$. The angular velocity matrix $\tilde{\boldsymbol{\Omega}}$ has only one independent component and the angular-velocity vector is $\boldsymbol{\Omega} = \Omega\hat{z}$. Under the rotation $\boldsymbol{x} = \boldsymbol{R}(t)\boldsymbol{y}$ the velocity $\boldsymbol{v}$ relative to the rotating frame is related to the velocity $\boldsymbol{u}$ relative to the inertial frame by $\boldsymbol{u} = \boldsymbol{R}(\boldsymbol{v} + \tilde{\boldsymbol{\Omega}}\boldsymbol{y}) = \boldsymbol{MR}\boldsymbol{y}$, or

$$\boldsymbol{v} = (\boldsymbol{R}^{\mathrm{t}}\boldsymbol{MR} - \tilde{\boldsymbol{\Omega}})\boldsymbol{y} \equiv \boldsymbol{L}\boldsymbol{y}, \tag{4.3}$$

where

$$\boldsymbol{L} = \begin{pmatrix} 0 & -(\zeta - \Omega) & 0 \\ \zeta - \Omega & 0 & -A/a_3 \\ 0 & a_3 A & 0 \end{pmatrix}. \tag{4.4}$$

The linearized equation (2.4) takes the form, in the rotating frame,

$$\boldsymbol{v}_t + 2\tilde{\boldsymbol{\Omega}}\boldsymbol{v} + ((\boldsymbol{L}\boldsymbol{x}) \cdot \nabla)\boldsymbol{v} + \boldsymbol{L}\boldsymbol{v} = -\nabla p, \tag{4.5}$$

where $\boldsymbol{v}, p$ now represent perturbations.

By contrast, Poincaré's solution for the simple flow of liquid inside a spheroid whose boundary is forced to precess about the vertical axis may be written, in the precessing frame, $\boldsymbol{v}_0 = \boldsymbol{A}\boldsymbol{x}$ where (Kerswell (1993))

$$\boldsymbol{A} = \begin{pmatrix} 0 & -1 & 0 \\ 1 & 0 & -(1+\eta)\mu \\ 0 & \mu & 0 \end{pmatrix}. \tag{4.6}$$

Here μ and η are parameters. The corresponding linearized equation is

$$\boldsymbol{v}_t + 2\hat{\boldsymbol{\Omega}}\boldsymbol{v} + ((\boldsymbol{A}\boldsymbol{x}) \cdot \nabla)\boldsymbol{v} + \boldsymbol{A}\boldsymbol{v} = -\nabla p, \tag{4.7}$$

where $\hat{\boldsymbol{\Omega}}$ is the angular-velocity matrix in the precessing frame. The formal analogy is obvious. Indeed, the matrix $\boldsymbol{L}$ of equation (4.4) can be made to coincide with the matrix $\boldsymbol{A}$ by appropriate choice of scaling: measure time in the unit $(\zeta - \omega)^{-1}$, let $a_3^2 = 1/(1+\eta)$ (which is the same as in Kerswell's paper) and let

$$\mu = \frac{2\sqrt{1+\eta}}{2+\eta}\frac{A}{\zeta} = \frac{2\sqrt{1+\eta}}{2+\eta}\frac{\sqrt{m_1^2 + m_2^2}}{\zeta} \tag{4.8}$$

(which is different). The angular-velocity matrix for the precessing boundary flow has two independent components and the angular-velocity vector (in the precessing frame) does not lie along the $\hat{z}$-axis of the container, or any principal axis for that matter. As a result, even in the limiting case when the figures become axially symmetric, the problem treated in the present paper is different from that of Kerswell (1993).

Kerswell shows that any such flow possesses two kinds of strain (his equation (1.1) is particularly transparent on this point). One is an elliptic strain due to the tilting of the plane of the fluid motion, and the other is due to a vertical shearing of the line of centres of the elliptical streamlines. Each of these separately can produce parametric instabilities, with different selection rules. These rules are usually described in terms of cylindrical coordinates, in which eigenfunctions of the unperturbed problem ($\mu = 0$) contain the factor $\mathrm{e}^{\mathrm{i}m\varphi}$, where φ is the azimuthal angle and m is an integer. In order for the elliptic instability, due to strain in the plane of motion, to arise from a resonance of two normal modes occurring in the limiting, axisymmetric problem, the m-values of the normal modes must differ by 2 (cf. Gledzer & Ponomarev 1992). In order for the instability due to strain perpendicular to the plane of motion to arise from a resonance of two normal modes occurring in the limit $\mu = 0$, the m-values of the normal modes must differ by 1. Note that these selection rules are necessary but not sufficient for these instabilities to occur at leading order in perturbation theory.

In figure 3, which shows that the elliptic instabilities are joined by further regions of instability, these further regions of instability can be related explicitly to the vertical shearing discussed by Kerswell. Consider in particular figure 3(c). The axially symmetric family is given here by $a_3 = 1$ so the roles of a_2 and a_3 are reversed in

comparison with the description above. The narrow region of instability intersects the line $a_3 = 1$ in a band centred (approximately) at $a_2 = 0.35$. For the unperturbed flow determined by the matrix $\boldsymbol{L}$, μ is small when (cf. equation (4.8)) the initial data represent a small departure from steady motion about the x_2-axis. This is exactly the situation to which figure 3(c) applies. Kerswell's analysis for small μ shows that the resonances with $\Delta m = 1$ are the candidates for instability. We have calculated frequencies for uniformly rotating spheroids under quadratic perturbations and find a resonance at $a_2 = 0.35846$ of modes for which $m = 1$ and $m = 2$. Since the calculation leading to figure 3(c) was done with a numerical value of μ which is small but not zero, the point 0.35846 (at $\mu = 0$) has broadened to a band. An understanding of the top unstable region appearing in figure 2(c) is obtained similarly. Again, at $\mu = 0$ we find that there is a resonance of $m = 1$ and $m = 2$ modes at $a_3 = 2.13896$ (note a_3 and a_2 have again reversed roles, so $a_2 = 1$). There is also a resonance of $m = 0$ with $m = 2$ for a prolate spheroid with $a_3 = 2.600$. Together, these two latter resonances account for the two unstable regions at the top of figure 2(c). Thus the analysis of Kerswell (1993) provides a qualitative understanding of the additional instabilities encountered in the present problem.

4.3. *Summary*

We have identified four different types of instability of our exact time-dependent ideal flow in ellipsoidal domains. When the underlying flow executes small oscillations about an equilibrium:

(a) there are instabilities reflecting the elliptic instability of the steady equilibria and due to the elliptical shape of the boundary cross-section;

(b) there is a further elliptical instability that occurs even if the boundary is axially symmetric due to the tilt of the vorticity vector (since the tilted planes on a spheroid intersect the boundary in ellipses);

(c) there are shearing instabilities (the streamlines are sheared normal to the flow direction); along with (b) these are analogous to instabilities of a precessing spheroid which were thoroughly investigated by Kerswell (1993).

Finally, when the underlying flow executes long-period, near separatrix oscillations:

(d) much of the parameter plane away from spherical symmetry is unstable. The wedges which occurred for small oscillations have widened to fill most of the space. Moreover, even the apparently stable parameter regions are interlaced with resonance filaments characteristic of near-separatrix periodic orbits.

Figures 2, 3 and 4 were based on an ordering of the semi-axes (equation (2.1)) fixing their relative sizes. This then requires imagining motions near each of the three coordinate axes in these three figures. This is convenient computationally, but makes the connections among the figures less than transparent. Figures 7(a) and 7(b) represent the calculations in a unified fashion. In these figures, all periodic orbits considered pass very close to the x_3-axis, but the semi-axes are no longer ordered in a fixed way, but are determined from the figure. The case when the equilibrium solution is about the intermediate axis (figures 4 and 5 above) is now represented by the region between the horizontal axis and the line $a_3/a_1 = a_2/a_1$. If these diagrams are overlaid on each other it is seen that for extreme shapes the near-equilibrium periodic orbits are mostly unstable, but in a neighbourhood of the origin, which represents a sphere, is there a significant region of stability. The points of instability in this near-sphere region are located between the abscissa and the 45° line $a_3 = a_2$ and represent the filamentary regions better seen in figure 5; the growth rates of these instabilities are quite small. The cross represents the ellipsoid with

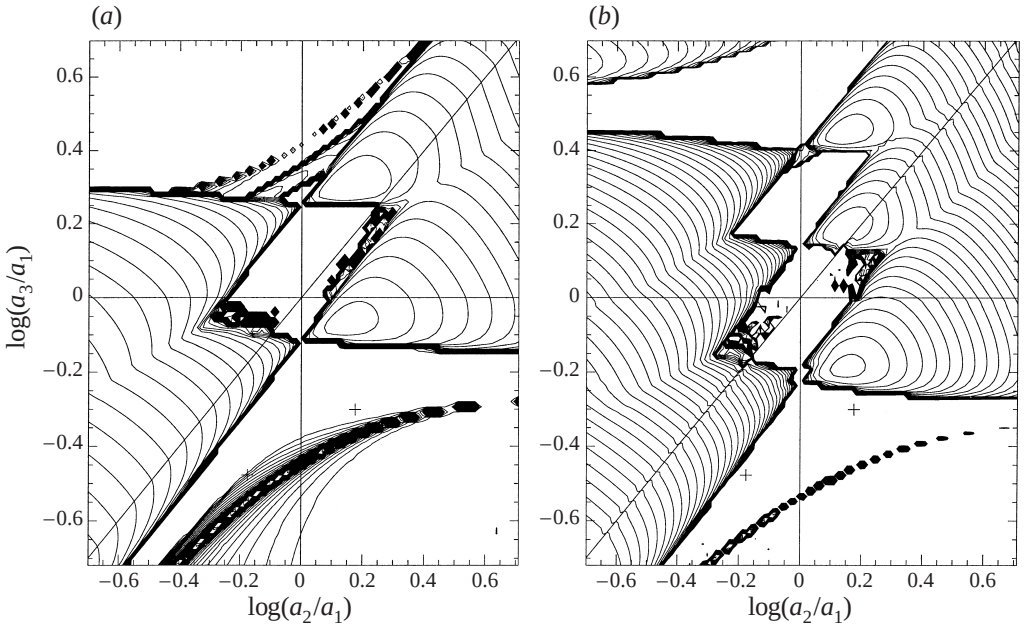

FIGURE 7. Unified diagram of growth rates (stable and unstable regions of parameter space) for (*a*) quadratic perturbations and (*b*) cubic perturbations. Initializing the vorticity primarily along the a_3-axis and varying a_3 and a_2 gives a full sampling of the oblate, prolate and near-separatrix cases discussed in the text. All orbits have been initialized with the same energy, providing initial data very close, but not identical to, those of figures 2–5. The parameters considered by Forster & Craik (1996) are denoted by a cross.

axes $(a_1, a_2, a_3) = (3, 2, 1)$ investigated by Forster & Craik (1996). Their investigation, which included but was not restricted to near-equilibrium orbits, led to a conclusion of instability for perturbations of asymptotically small spatial scale.

We would like to thank A. Neishtadt who brought to our attention the stability results for near-separatrix periodic orbits as discussed in § 3.3. The research reported here was supported in part by the National Aeronautics and Space Administration under grant NASA NAG5-1485 (J. A. B.) and by the National Science Foundation under grant DMS 9500804 (K. I. S. and N. R. L.).

REFERENCES

BAYLY, B. J. 1986 Three-dimensional instability of elliptical flow. *Phys. Rev. Lett.* **57**, 2160–2171.

BUSSE, F. 1968 Steady flow in a precessing ellipsoidal shell. *J. Fluid Mech.* **33**, 739–752.

CHURCHILL, R. C., PECELLI, G. & ROD, D. L. 1980 Stability transitions for periodic orbits in Hamiltonian systems. *Arch. Rat. Mech. Anal.* **73**, 313–347.

FORSTER, G. K. & CRAIK, A. D. D. 1996 The stability of three-dimensional time-periodic flows with ellipsoidal stream surfaces. *J. Fluid Mech.* **324**, 379–391.

GLEDZER, E. B., NOVIKOV, YU. V., OBUKHOV, A. M. & CHUSOV, M. A. 1974 An investigation of the stability of liquid flows in a three-axis ellipsoid. *Isv. Acad. Sci. USSR Atmos. Ocean. Phys.* **10**, 69–71.

GLEDZER, E. B. & PONOMAREV, V. M. 1977 Finite-dimensional approximation of the motions of an incompressible fluid in an ellipsoid cavity. *Isv. Ocean. Phys.* **13**, 565–589.

GLEDZER, E. B. & PONOMAREV, V. M. 1992 Instability of bounded flows with elliptical streamlines. *J. Fluid Mech.* **240**, 1–30.

GUCKENHEIMER, J. & MAHALOV, A. 1992 Instability induced by symmetry reduction. *Phys. Rev. Lett*. **68**, 2257–2260.

KERSWELL, R. R. 1993 The instability of precessing flow. *Geophys. Astrophys. Fluid Dyn.* **72**, 107–144.

KERSWELL, R. R. 1999 Secondary instabilities in rapidly rotating fluids: inertial wave breakdown. *J. Fluid Mech.* **382**, 283–306.

KNOBLOCH, E., MAHALOV, A. & MARSDEN, J. E. 1994 Normal forms for three-dimensional parametric instabilities in ideal hydrodynamics. *Physica* D **73**, 49–81.

LEBOVITZ, N. 1989 The stability equations for rotating, inviscid fluids: Galerkin methods and orthogonal bases. *Geophys. Astrophys. Fluid Dyn.* **46**, 221–243.

LEBOVITZ, N. & LIFSCHITZ, A. 1996 New global instabilities of the Riemann ellipsoids *Astrophys. J.* **458**, 699–713.

LEBOVITZ, N. R. & SALDANHA, K. I. 1999 On the weakly nonlinear development of the elliptic instability. *Phys. Fluids* **11**, 3374–3379.

LIFSCHITZ, A. & FABIJONAS, B. 1996 A new class of instabilities of rotating fluids. *Phys. Fluids* **8**, 2239–2241.

MALKUS, W. V. R. 1989 An experimental study of global instabilities due to the tidal (elliptical) distortion of a rotating elastic cylinder. *Geophys. Astrophys. Fluid Dyn.* **48**, 123–134.

MASON, D. M. & KERSWELL, R. R. 1999 Nonlinear evolution of the elliptical instability: an example of inertial wave breakdown. *J. Fluid Mech.* **396**, 73–108.

MORRISON, P. 1998 Hamiltonian description of the ideal fluid. *Rev. Mod. Phys.* **70**, 467–521.

PIERREHUMBERT, R. T. 1986 Universal short-wave instability of two-dimensional eddies in an inviscid fluid. *Phys. Rev. Lett*. **57**, 2157–2159.

POINCARÉ, H. 1910 *Bull. Astron.* **27**, 321–356.

ROBERTS, P. H. & STEWARTSON, K. 1965 On the motion in a liquid in a spheroidal cavity of a precessing rigid body II. *Proc. Camb. Phil. Soc.* **61**, 279–288.

WALEFFE, F. 1989 The 3D instability of a strained vortex and its relation to turbulence. PhD Thesis, Massachusetts Institute of Technology.

WALEFFE, F. 1990 On the three dimensional instability of strained vortices. *Phys. Fluids* A **2**, 76–80.